

Performance optimization of MASnI_3 perovskite solar cells: Insights into device architecture

Prithick Saha ^{a,b,*}, Sangeeta Singh ^a, Sanjib Bhattacharya ^c

^a Microelectronics and VLSI Design Lab National Institute of Technology, Patna, 800005, Bihar, India

^b Dream Institute of Technology, Department of Electronics and Communication Engineering, Kolkata, 104, West Bengal, India

^c UGC-HRDC and Composite Materials Research Laboratory, University of North Bengal, India



ARTICLE INFO

Keywords:

Lead-free
 MASnI_3
 Solar cell capacitance simulator (SCAPS)
 Perovskite solar cells (PSCs)
 WS_2

ABSTRACT

Recent research has focused an extensive amount of attention on the lead-free substance lead-free methylammonium tin(Sn) tri-iodide (MASnI_3), which has emerged as a highly potential absorber layer in the structure of the device. Because it has a larger visible absorption spectrum and a shorter band gap of 1.3 eV than the lead halide perovskite, MASnI_3 is a potential alternative to MAPbX_3 . Through numerical simulation, the different parameters on the device performances are fully investigated. We achieved an open-circuit voltage (V_{oc}) of 0.93 V, a short-circuit current density (J_{sc}) of 22.20 mA/cm², a fill factor (FF) of 78.81 %, and a power conversion efficiency (PCE) of 16.39 % using the optimised conditions. It demonstrates the huge potential of recently created lead-free perovskite solar cells and opens up a large dimension of opportunities for the creation of novel perovskite solar cells with a variety of photovoltaic applications. The amalgamation of the Tungsten Disulfide (WS_2) material layer between the electron transport layer (ETL) and the absorber layer raised the device module's power conversion efficiency to 20.36 %.

1. Introduction

Researchers in photovoltaics have been working nonstop to advance the field, and increasing interest in improved optical and electrical performance, affordable methods and adaptability has been shown in a number of developing solar systems. Perovskite solar cells (PSCs), a recent development among these technologies that has the potential to produce a cheap and solar cell with high efficiency, have attracted the interest of the green energy sector. In addition to having a straight band gap, a relatively low bond state energy, huge hole-electron diffusion length, a tremendous light absorption, a lofty tolerance to defects, and efficient bipolar carrier transport, perovskite is utilised as an absorber layer in solar cell systems [1–3]. Its power conversion efficiency (PCE) has enhanced from 3.2 % [4] to 25.2 % [5] as a result of these characteristics. The ABX_3 perovskite structure, which combines methylammonium (CH_3NH_3^+) (MA), formamidinium ($\text{NH}_2\text{CHNH}_2^+$) (FA), and cesium (Cs^+) in the A-cation site, lead (Pb) in the B-cation site, and iodine (I) and bromine (Br) in the X-anion site, has so far presented to be the most flourishing composition in perovskite [6]. Wide band gaps in Pb-free perovskite active materials make them viable replacements for harmful lead(Pb)-containing perovskites. Methylammonium tin iodide (MASnI_3 : 1.3 eV), cesium tin iodide (CsSnI_3 : 1.22 eV), and formamidinium tin iodide (1.41 eV) are a few examples [7] [-] [9]. Tin(Sn)-based perovskites are receiving grown recognition in the scientific community on account of their characteristics, as it is comparable to those of Pb-based halide perovskites with huge efficiency. After all, a significant issue that needs to be solved is how

* Corresponding author. Microelectronics and VLSI Design Lab National Institute of Technology, Patna, 800005, Bihar, India.
 E-mail address: prithicks.ph21.ec@nitp.ac.in (P. Saha).

these devices degrade in the ambient environment. Lead-free MASnI_3 -based PSCs with PCE of 6 % was claimed by Neol et al. [10]. The Pb-based PSCs, it is true that Sn-based PSCs device have had stability issues. Sn-based perovskites often exhibit lower long-term stability and are more susceptible to deterioration, particularly when exposed to heat, humidity, and light. This impermanence may cause performance to suffer and restrict their useful applications [11].

Nilesh, Jaiswal et al. [12] led the development of environmentally kind Cs_2SnI_6 double perovskite thin-film solar cells by solution processing. The comparative study of $\text{Cu}_2\text{ZnSn}(\text{S}_x\text{Se}_{1-x})_4$ nanoparticles for solar cells, spanning from chemical synthesis to device fabrication, was conducted by Prabhu, Sudheendra et al. [13]. Subudhi, Poonam et al. [14] spearheaded the investigation of hybrid electron transport layer-based perovskite solar cells as an essential path towards enhancing efficiency. Pandey, Nivedita et al. [15] carried out the large-scale, low-cost, surfactant-free hydrothermal synthesis and characterisation of CZTS ink for solar applications. Kumari, Dolly et al. [16] designed and manufactured Cs_2SnI_6 perovskite solar cells using only inorganic transport materials. The analysis of the performance parameters of stable and environmentally friendly perovskite solar cells was conducted by Shukla, Raghvendra et al. [17]. Kumar, A. et al. [18] investigated how to improve the performance of phenylethylammonium-formamidinium tin iodide perovskite solar cells by comparing different electron transport layer (ETL) and hole transport layer (HTL) materials. Shukla, Raghvendra et al. [19] conducted a thorough investigation into the design viewpoint, fabrication, and performance analysis of formamidinium tin halide perovskite solar cells. Chandel, Rashi et al. [20] enhanced ethylammonium-substituted tin-based perovskite solar cells with different hole transport materials to achieve high efficiency and environmental approachability.

Neol et al. [10] reported MASnI_3 based n-i-p hetero-junction PSCs with power conversion efficiency 6 %. Afterwards Feng Hao et al. [21] reported power conversion efficiency 5.23 %, 5.48 %, 5.73 % and 4.27 % respectively. Tin based PSCs, Feng Hao et al. [22] provided an encouraging efficiency of 5.44 %. Fengzhu Li et al. [23] improved power conversion efficiency 6.83 %. The most acceptable approach for adding spin-orbit coupling (SOC) characteristics onto an effective GW system, Umari et al. [24] highlighted the existing research on the optoelectronic characteristic of MASnI_3 . Due to the Sn-based perovskites' higher crystallisation rate, the film-forming methods designed for Pb-based perovskites are no longer effective [26]. As a result, many investigations have demonstrated the impact of solvents on the crystallisation of MASnI_3 perovskite films [27]. Compared to MAPbI_3 -based devices, the MASnI_3 PSCs module possesses higher carrier density & equivalent recombination rates, according to transient photo-voltage decay and charge extraction tests [25]. In order to create immense-quality tin(Sn)-based perovskite thick films, numerous techniques have been suggested [27,28]. A good-quality, thin film with significantly improved stability was created after a 10-min thermal annealing. The films held their stability in both light and dark conditions after 90 min in the air. An electron transport layer (ETL)(titanium dioxide (TiO_2)) is usually surrounded by a perovskite layer($\text{CH}_3\text{NH}_3\text{SnI}_3(\text{MASnI}_3)$), which acts as the absorber (active layer), and is followed by a hole transport layer (HTL)(2,2',7,7'-Tetrakis[N,N-di(4-methoxyphenyl)amino]-9,9'-spirobifluorene- Spiro-oMeTAD). The ETL and HTL's morphology has an impact on the PSCs' stability and effectiveness. Before being gathered, the carriers produced by photography pass through these layers. In the present work, we give a thorough numerical analysis of a low bandgap antimony-based perovskite with transparent conductive oxide (TCO)/ $\text{TiO}_2/\text{MASnI}_3/\text{Spiro}-\text{oMeTAD}/\text{Au}$ in a n-i-p heterojunction configuration. To create the highest performing device module, we design a simulation model and optimise the materials parameters. The MASnI_3 device architecture, which is likely related to perovskite solar cells, has many obstacles in its real-world application. These include challenges with reproducibility resulting from variations in film characteristics, scalability when moving to large-scale production, stability issues brought on by the degradation susceptibility of perovskite material, cost considerations associated with fabrication and encapsulation, and environmental concerns, particularly those pertaining to the toxicity of specific elements like lead and tin. Refining fabrication techniques, improving material stability through encapsulation techniques and compositional adjustments, creating scalable manufacturing processes, cutting costs through efficiency improvements and alternative materials, and addressing environmental concerns with eco-friendly practices and lead-free perovskite formulations are just a few of the strategic approaches needed to overcome these challenges. By overcoming these challenges, the MASnI_3 architecture may be able to live up to its potential of providing effective, affordable, and sustainable.

To overcome major obstacles and progress the technology, lead-free perovskite solar cell complications necessitate a multipronged strategy. MASnI_3 architectures will be more durable and reliable if stability augmentation via creative encapsulation strategies and compositional optimization is prioritised. Simultaneously, improving manufacturing techniques and putting strict quality control measures in place will guarantee reproducibility in large-scale production, making the shift from lab-scale research to commercial viability easier. Efficient manufacturing techniques and the investigation of substitute materials can alleviate cost concerns, promoting financial viability and extensive implementation. In addition, a dedication to environmental sustainability means creating environmentally friendly procedures and searching for lead-free perovskite formulations that minimise environmental effect while optimising energy efficiency. Adopting these tactics will accelerate the development of lead-free perovskite solar cells.

In order to create a non-toxic, incredibly effective, and stable PSC, we carried out computational modelling and simulation of Pb-free perovskite solar cells using perovskite. The electron transport layer materials added carbon 60 (C_60), CdS (Cadmium sulfide), IGZO (Indium gallium zinc oxide), PCBM (fullerene derivative [6,6]-phenyl-C₆₁-butyric acid methyl ester), and ZnO (Zinc oxide) further improved.

There are four sections in this article. In Section II, the model and its validation are fully described, along with the outcomes of the experiments. In Section III, the results and analysis of different parameters are discussed. This article's conclusions are presented in Section IV.

2. Device model

We used Solar Cell Capacitance Simulator (1-D) software version 3.3.10 (ELIS, University of Gent, Belgium) to simulate the conduct

of PSCs utilising various thicknesses and band gap energies of the tin-based perovskite layer [29]. The simulation was run under AM 1.5 G 1 solar light at a working temperature of 300 K.

In this study, solar cell capacitance simulator (SCAPS) has been deployed for device modeling. The electron continuity equations eqns. (1) and (2), along with Poisson's eqn. (3) and the constitutive eqns. (4) and (5)

$$\frac{dJ_n}{dx} = G(x) - U_n \quad (1)$$

$$\frac{dJ_p}{dx} = G(x) - U_p \quad (2)$$

$$\frac{d}{dx} \left(\epsilon_r \epsilon_0 \frac{d\psi}{dx} \right) = -\frac{q}{\epsilon} (p - n + N_D^+ - N_A^- + p_t - n_t) \quad (3)$$

$$J_n = -\frac{n\mu_n}{q} \frac{dE_{Fn}}{dx} \quad (4)$$

$$J_p = +\frac{p\mu_p}{q} \frac{dE_{Fp}}{dx} \quad (5)$$

where, ϵ = semiconductor permittivity, ψ = electrostatic potential, N_D^+ and N_A^- = the densities of ionized donors and acceptors, n and p = free carrier concentrations, J_n and J_p = the electron and hole current densities, and G = generation rate.

Md Uddin et al. perform a thorough investigation using Density Functional Theory (DFT) and SCAPS-1D simulation techniques to examine the combined optoelectronic and photovoltaic properties of lead-free $\text{Cs}_2\text{AgBiBr}_6$ double perovskite solar cells [35]. Density Functional Theory (DFT) was utilised in the study of heavy thallium perovskites TlGeX_3 ($X = \text{Cl}, \text{Br}$, and I) for optoelectronic and thermoelectric applications by Bouhmaidi, Soukaina et al. [36]. Hossain, M. Khalid et al. conducted a thorough investigation of the combined optoelectronic and photovoltaic characteristics of lead-free CsSnI_3 perovskite-based solar cells, utilising SCAPS-1D simulations and Density Functional Theory (DFT) calculations [37]. Hossain, M. Khalid et al. carried out a comprehensive analysis of various combinations of electron transport layer (ETL) and hole transport layer (HTL) for the purpose of designing and simulating high-performance lead-free CsSnCl_3 -based perovskite solar cells [38]. Hossain, M. Khalid et al. studied the design and simulation of $\text{Cs}_2\text{BiAgI}_6$ double perovskite solar cells using different electron transport layers for efficiency enhancement [39]. By using a combination of Density Functional Theory (DFT), SCAPS-1D simulations, and wxAMPS frameworks, an efficient $\text{Cs}_2\text{BiAgI}_6$ -based perovskite solar cell with varying charge transport layers was optimised. The author of this study is Hossain, M. Khalid et al. [40]. Numerical analysis was performed using Density Functional Theory (DFT) and SCAPS-1D to explore the influence of various charge transport layers on CsPbBr_3 perovskite solar cells. This investigation provided insights into the performance enhancement strategies, led by Hossain, M. Khalid et al. [41].

The PSCs suggested architecture is concluded in Fig. 1. Table 1 provides the material characteristics of each layer. The entire data was derived from published studies [30–34]. Defect density have been treated at the interfaces while defects with a Gaussian distribution have been considered in the perovskite absorber layer. The defect density at the HTL and ETL interfaces with the active layer

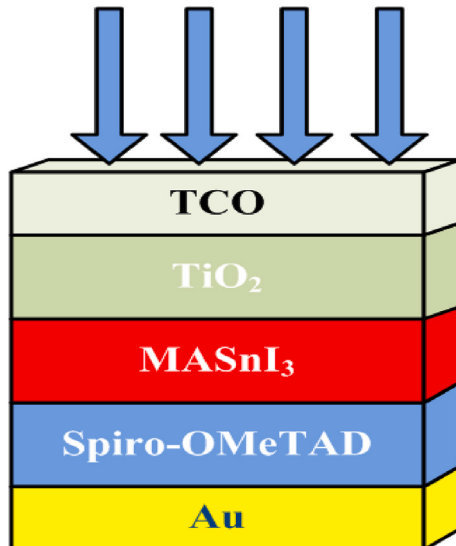


Fig. 1. MASnI_3 based PSCs device architecture.

has been estimated to be 1.00×10^{15} and $1.00 \times 10^{15} \text{ cm}^{-3}$. At the bulk and interfaces, the capture cross section for holes and electrons are assumed to be $2.00 \times 10^{-14} \text{ cm}^2$ and $2.00 \times 10^{-14} \text{ cm}^2$, respectively. All of the simulations were run at 300 K. The selection of metal work functions for the front transparent conductive oxide (TCO) and back contact (usually gold, Au) is crucial in simulations involving solar cells or optoelectronic devices. Transparent conducting electrodes (TCO) are made of materials such as indium tin oxide (ITO), fluorine-doped tin oxide (FTO), or aluminum-doped zinc oxide (AZO). Their work function values usually fall between 4.5 and 5.5 eV. Due to its exceptional conductivity and stability, gold (Au) is frequently employed as the back contact material. Its work function ranges from roughly 5.1 eV–5.4 eV. Accurate specification in simulations is necessary since these work function values impact the energy barrier height at the metal-semiconductor interface, which in turn affects the efficiency of charge carrier injection and extraction within the device.

A comparison with the experimental work described by has been made in order to assure a self-consistent device model [10]. The I-V curve is approximately similar to the experimentally reported device, as seen in Fig. 2. Our simulated current density(J_{sc}) of 16.5 mA/cm^2 , Voltage (V_{oc}) of 0.73 V , Fill factor(FF) of 57.46% and Power conversion efficiency(PCE) of 7.03% is nearly identical to the experimentally reported current density(J_{sc}) of 16.8 mA/cm^2 , Voltage (V_{oc}) of 0.88 V , Fill factor(FF) of 42.00% and Power conversion efficiency(PCE) of 6.45% illustrating the in Fig. 2. Fig. 3 (a) and (b) depicts the MASnI₃-device module energy band alignment. Using MASnI₃ based device module, we explored the effects of several areas on the device's performance. Table 2 indicates the most significant parameters and shows an error for each parameter.

3. Results and analysis

3.1. Doping Concentration's influence on perovskite active layer

The electrical behaviour of the PSCs is mostly ascertained by the dopant density of perovskite materials, and this has a massive impact on the behavior of the solar cell. In the presence of airborne contaminants, CH₃NH₃SnX₃ (where X = Cl, Br, or I) is troubled; the Sn²⁺ ion will quickly oxidise into the better standing Sn⁴⁺ analogue, which functions as a p-type dopant within the substance in the self-doping process [21]. The act of the PSCs can be influenced by the acceptor dopant density (N_A) of the MASnI₃ layer; for this reason, CH₃NH₃SnI₃ layers with N_A values between 10^{14} cm^{-3} and 10^{17} cm^{-3} are taken into consideration and the remaining layer properties are the same as those of the currently optimised device, and the outcome is presented in Fig. 4.

At a dopant concentration of 10^{16} cm^{-3} , the best performance was attained. Due to a rise in electric field in the bulk region, which effectively separated exciton, an increase in performance was seen with a drop in dopant concentration. Because of the rise in scattering, which results in undesirable charge carrier recombination, performance below 10^{16} cm^{-3} decreased. The device performs according to its most effective i.e. $V_{oc} = 0.73 \text{ V}$, $J_{sc} = 16.69 \text{ mA/cm}^2$, FF = 64.45% and PCE = 7.87% at 10^{16} cm^{-3} doping concentration.

3.2. Influence of perovskite active layer defect density

All materials by their very nature include defects. A device free of defects is practically unattainable. As a result, a details analysis of the influence of defect order density on MASnI₃ device effectiveness is essential. Normal defect density is influenced by the film's

Table 1

Materials characteristics used in the PSC based on the MASnI₃ device module [30-34].

Parameters	Spiro-OMeTAD	MASnI ₃	TiO ₂	TCO	WS ₂
Thickness (T)nm	200	350	30	500	20
Band gap (E _g) eV	3.17	1.3	3.2	3.5	1.8
Electron affinity (χ) eV	2.05	4.17	4.26	4	3.95
Dielectric constant (ε _r)	3	8.2	9	9	13.6
CB effective (N _c)1/cm ³	2.20×10^{18}	1.00×10^{18}	2.00×10^{18}	2.20×10^{19}	1.50×10^{18}
VB effective (N _v) 1/cm ³	1.80×10^{19}	1.00×10^{18}	1.80×10^{19}	1.80×10^{19}	1.80×10^{19}
Electron mobility (cm ⁻² /V·s)	2.00×10^{-4}	1.6	20	20	100
Hole mobility (cm ⁻² /V·s)	2.00×10^{-4}	1.6	10	10	100
Defect density (1/cm ³)	1.00×10^{15}	4.50×10^{17}	1.00×10^{15}	1.00×10^{15}	1.00×10^{15}
Shallow donor density (N _D) (1/cm ³)	0	0	1.00×10^{16}	2.00×10^{19}	1.00×10^{18}
Shallow acceptor density (N _A) (1/cm ³)	2.00×10^{19}	3.20×10^{15}	0	0	0

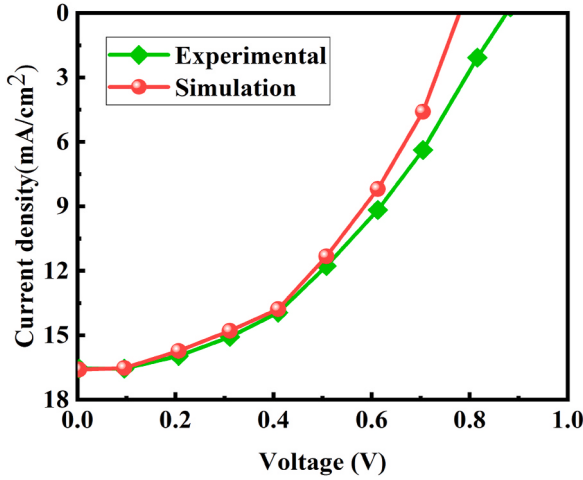


Fig. 2. J-V curve measurement of the practical simulation architecture implementing the simulation PSCs device [10].

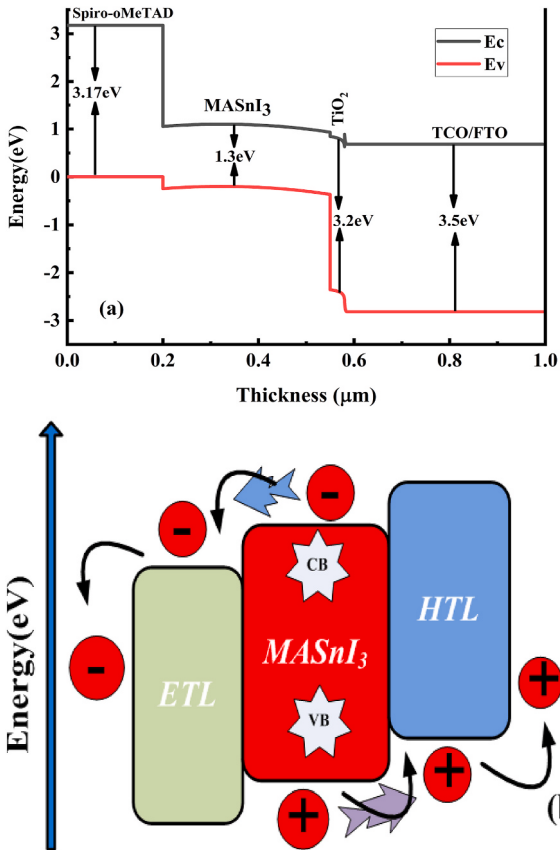


Fig. 3. (a) MASnI₃ PSCs energy band diagram. (b) Device operation mechanism.

crystallinity architecture, therefore by controlling these elements, Ju et al. [42] revealed that a single crystal may defect density of 10^{10} 1/cm³. While other variables remained fixed, the active layer defect density was changed from 10^{14} – 10^{19} cm^{−3}.

According to Fig. 5, a decrease in the charge carrier's diffusion length leads to an increase in trap-assisted recombination growth, which causes a considerable fall in efficiency(PCE) from 9.6 % to 0.0 % with an gain the defect density also leads to decrease others parameters. Even with a further reduction in N_t from 10^{15} cm^{−3}– 10^{14} cm^{−3}, the performance of the cell only slightly improves. We chose a defect density of 10^{15} cm^{−3} as an optimised value since it is exceedingly challenging to achieve an experiment with a low N_t of

Table 2

Primary performance variables and the error between simulation and Experimental results.

	PCE(%)	J_{sc} (mA/cm 2)	V_{oc} (V)	FF(%)
Simulation	7.03	16.5	0.73	57.46
Experimental	6.4	16.8	0.88	42.0
Error	0.63	0.3	0.15	15.46

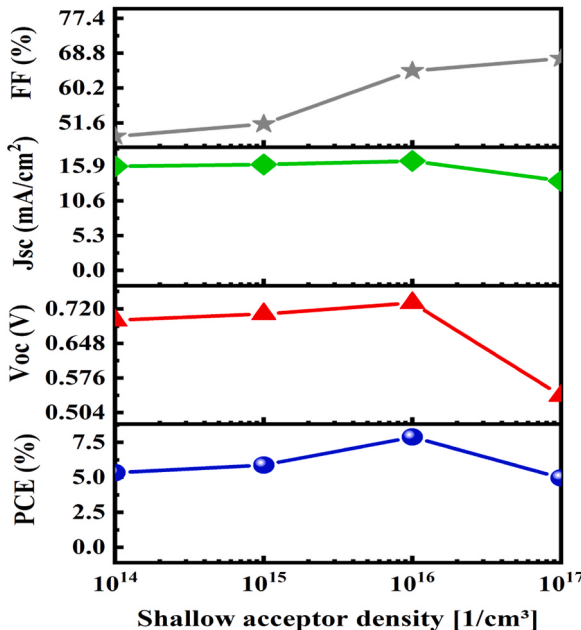


Fig. 4. Doping concentration has an impact on the device's performance.

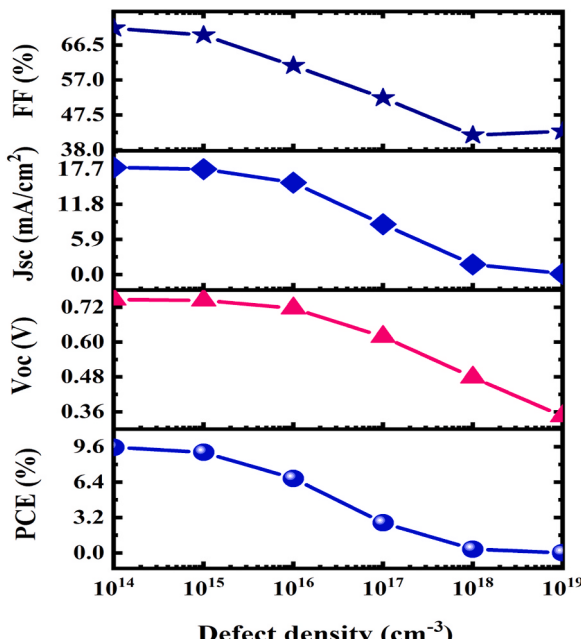


Fig. 5. Performance of the device is affected by the density of defects in the absorber layer.

10^{14} cm $^{-3}$, and all the values of J_{sc} , V_{oc} , FF, and PCE roughly reach their maximum with this defect density.

3.3. Influence of perovskite active layer thickness

The active perovskite absorber layer thickness has a significant effect on the cell's performance [43]. Numerical simulations are also used to investigate how the thickness of the MASnI_3 layer affects the performance of the cell. In these simulations, the thickness is considered to range from 100 to 1000 nm. Fig. 6 illustrates the simulation observations. The graph indicates that as MASnI_3 layer thickness rises, V_{oc} , J_{sc} , & power conversion efficiency values increase. The J_{sc} value improves because more of the photons will be received by the layer while the absorber layer thickness increases. As observed in Fig. 6, all of those results become saturated as the thickness reaches and exceeds 800 nm. The perovskite layer is 800 nm thick and achieves a $V_{oc} = 0.75$ V, $J_{sc} = 20.44$ mA/cm 2 , FF = 74.93 % and PCE = 11.55 %, improving cell performance over the baseline cell performance.

3.4. Impact of ETL in PSCs performance

For enhanced performance of devices in PSC, a choice of ETMs be able to made utilising a precise optimization technique. To attain the highest possible solar cell factors, we used C60, CdS, ZnO, IGZO and PCBM as ETMs in the contemporary simulation explore. In addition, the simulation research of the PSCs uses an thorough electron transport materials thickness of 30 nm. Table 3 utilises the electron transport materials input parameters along with their individual electrical properties. The ETL materials proposed in this paper C60 [46], CdS [47], IGZO [44,45], ZnO [48], and PCBM [44,49] are practical and have been confirmed in the studies that have been published. Fig. 7 illustrates that the conduction band (CB) level of nearly all investigated electron transport layer materials is higher than that of the MASnI_3 perovskite.

The contrast linking the ETL CB level besides the perovskite CB level is recognized as the conduction band offset (CBO). If the ETL's CB level is lower than the perovskite's, there will be an energy peak at the ETL/perovskite interface. The mass energy need for carrier recombination is equal to the band gap of the perovskite, so the mass energy is higher than that computed by energy cliff, which surely will improve the performance of the cell. The energy increase that forms at the ETL/perovskite interface creates a barrier for the photo-generated electrons in other ETL materials. Additionally, it is demonstrated that a small-range energy surge has a bigger impact on the carrier recombination rate than it does on the mobility of photo-generated electrons [50]. In Fig. 8, the J-V parameter for the MASnI_3 -based PSC device is simulated under idealised preconditions for various ETMs. Because the PSC device has superior carrier mobility, the I-V curve for the simulated ETMs yields identical characteristics for all the ETMs except ZnO.

According to the computational results, MASnI_3 's intrinsic electronic structure and high electron mobility enable it to exhibit significant electron transport capabilities, which makes it a good choice for use as an electron transport layer (ETL) in electrical devices. However, it seems to have limited performance as a hole transport layer (HTL), either because of less favourable energy levels or poorer hole mobility. Although doping MASnI_3 might boost hole transport somewhat, it might not greatly improve electron conduction. These findings highlight the principal function of MASnI_3 in electrical devices as an ETL, highlighting its potential to promote electron transport while highlighting difficulties with hole conduction. The combination of MASnI_3 as an electron transport layer (ETL)

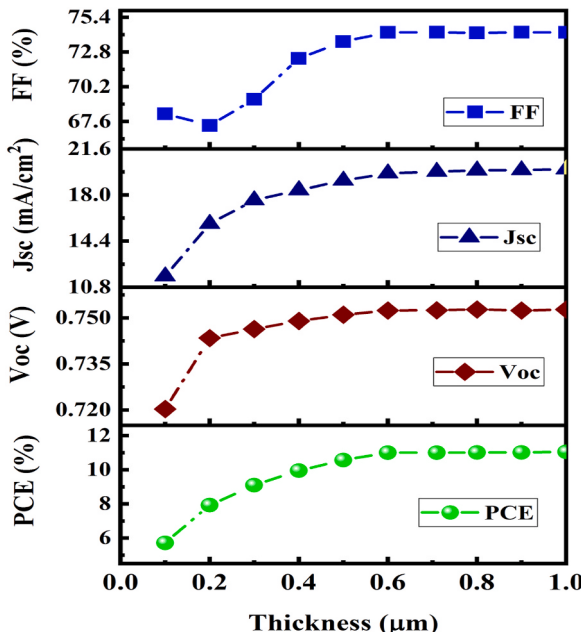
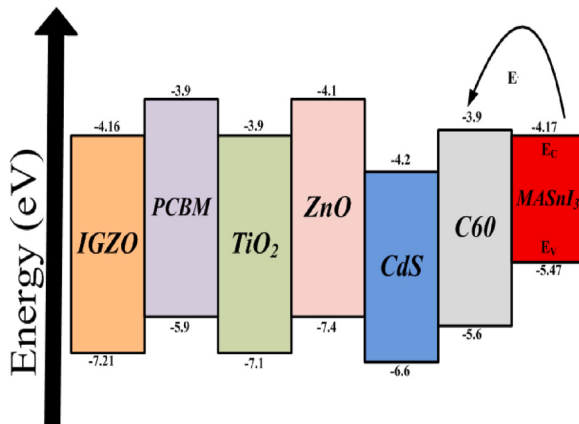
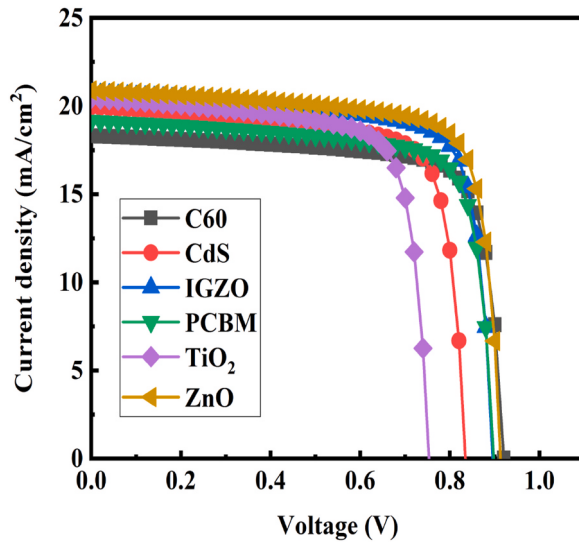


Fig. 6. Influence of absorber layer thickness on efficiency of solar cells.

Table 3

Various Electron Transporting Materials simulation input and material properties [44–49].

Parameters	C60	CdS	IGZO	PCBM	ZnO
E_g (eV)	1.7	2.4	3.05	2	3.3
χ (eV)	3.9	4.2	4.16	3.9	4.1
ϵ_r	4.2	10	10	3.9	9
$N_e(\text{cm}^{-3})$	8×10^{19}	2.2×10^{18}	5×10^{18}	2.5×10^{21}	4×10^{18}
$N_v(\text{cm}^{-3})$	8×10^{19}	1.8×10^{19}	5×10^{18}	2.5×10^{21}	1×10^{19}
$\mu_n(\text{cm}^2/\text{VS})$	0.08	100	15	0.2	100
$\mu_p(\text{cm}^2/\text{VS})$	0.0035	25	0.1	0.2	25
$N_d(\text{cm}^{-3})$	2.6×10^{18}	1×10^{17}	1×10^{18}	2.93×10^{17}	1×10^{18}
$N_a(\text{cm}^{-3})$	0	0	0	0	0
$N_t(\text{cm}^{-3})$	1×10^{17}	1×10^{15}	1×10^{15}	1×10^{15}	1×10^{15}

**Fig. 7.** ETL materials and the MASnI_3 perovskite have their bands alignment.**Fig. 8.** J-V curve variation for multiple ETMs in the MASnI_3 -based PSC obtained.

with other materials serving as hole transport layers (HTLs) in solar cell layouts has proven to offer superior properties, as evidenced by recent research. Device stability and efficiency have improved with the use of MASnI_3 as an ETL in conjunction with materials such as PTAA or spiro-OMeTAD as HTLs. In order to supplement the advantageous electron transport properties of MASnI_3 , researchers leveraged the superior hole transport features of alternative HTL materials to minimise recombination at the ETL/HTL interface and improve charge extraction. This combination has demonstrated efficacy in enhancing perovskite solar cell topologies and propelling

solar energy technologies forward, as seen by enhanced device stability and overall performance.

As can be shown in Fig. 9, the simulated ETM of ZnO overtake a slightly better QE than the other ETMs, whereas the other ETMs exhibit QE constant over the simulated spectrum limits. The ETM of ZnO has achieved a hugely improved J_{sc} value of 20.88 mA/cm^2 , as can be apparent. Due to the carriers' suitable mobility in the PSCs module, ETMs like C60, PCBM, IGZO, ZnO and CdS offer an imperceptible value of J_{sc} . The ZnO ETM device enables to get an improved PCE of 14.77 %. Table 4 bring an overview of the simulated PSC characteristics for particular ETMs.

3.5. Influence of interface defect density

The efficiency of the MASnI_3 device is really influence by the interface layer of PSCs. The MASnI_3 device was used to scrutinize the influences of interface defect density on the perovskite solar cells behavior more defect density result in lower layer quality and greater recombination rates [51]. In order to analyse how the density of interface layer defects affects PSCs behavior, we considered that the defect of Interface Layer-1 and Interface Layer-2 range between 10^{10} and 10^{17} 1/cm^3 .

The influence of interface layer defect on efficiency is seen in Fig. 10. These graphs indicate that improving V_{oc} and J_{sc} and efficiency is going to improve by decreasing the interface layer's defect density. Due to enhanced recombination at the interface, PCE reduced from 16.4 % to 14.8 % as defect density grew. Therefore, for high-performance devices, It is necessary to have a flat defect at the illuminated part contact. Controlling the density of interface defects is possible using interface engineering. We impart the optimised interface defect density of $10^{10} (\text{1/cm}^3)$.

3.6. Influence of addition of an InterLayer

The technique used in preventing recombination is by adding an interlayer layer between ZnO (ETL) and MASnI_3 -layer. It has been claimed that a number of transition metal dichalcogenides (TMDs) can be utilised just as a layer in between to increase PSCs performance[52] [-] [54]. In this subsection, we investigated the solar cell's effectiveness with WS_2 added between the ZnO & MASnI_3 -layer. Table 1 summarises the WS_2 characteristics.

The tungsten disulfide (WS_2) material layer acts as a passivation layer for the perovskite active layer, which is how it primarily contributes to the device's increased power conversion efficiency. With the help of WS_2 , perovskite surface defects are successfully passivated, reducing non-radiative recombination processes and improving charge carrier extraction and transport inside the device. Moreover, WS_2 can function as a barrier layer, keeping oxygen and moisture from diffusing into the perovskite layer and enhancing the device's long-term stability. In addition, the advantageous electrical characteristics of WS_2 , like its elevated electron mobility, facilitate the effective extraction of electrons from the perovskite layer, hence augmenting the overall efficiency and performance of the device. The WS_2 energy level reduces the barrier potential and eliminates electron interaction that occurs between the active layer and ZnO , allowing for an efficient transfer of charge carriers. Therefore a drop in series-resistance and a shift in V_{oc} from 22.20 to 24.75 V, the PCE of the enhanced device grew from 16.39 % to 20.37 %. By creating a WS_2 - ZnO composite using the techniques described in the literature now in existence, a pinhole-free inter-layer perchance added practically [55,56]. Fig. 11 illustrated the J-V characteristics after and before the optimization. The energy band equilibrium of proposed device is blocked-out in Fig. 12. The best PSCs effectiveness is noted with $V_{oc} = 0.97 \text{ V}$, $J_{sc} = 24.75 \text{ mA/cm}^2$, FF = 84.66 %, and PCE = 20.37 % represent the ideal PSCs performance.

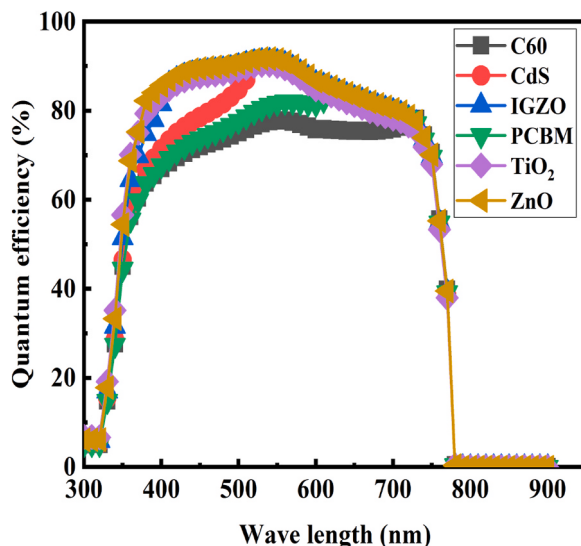


Fig. 9. Effect of various ETMs to investigate QE properties across wavelength in MASnI_3 -based PSC structures.

Table 4MASnI₃-based device module outcomes to multiple Electron Transporting Materials.

Parameters	C60	CdS	ZnO	TiO ₂	PCBM	IGZO
V _{oc} (V)	0.92	0.83	0.91	0.75	0.89	0.89
J _{sc} (mA/cm ²)	18.31	19.96	20.88	20.44	19.16	20.70
FF(%)	77.70	75.82	77.40	74.93	76.71	76.74
PCE(%)	13.09	12.65	14.77	11.55	13.21	14.24

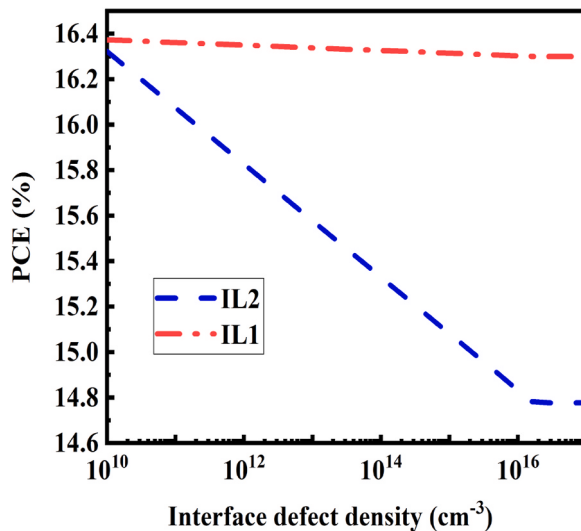


Fig. 10. Interface defect density.

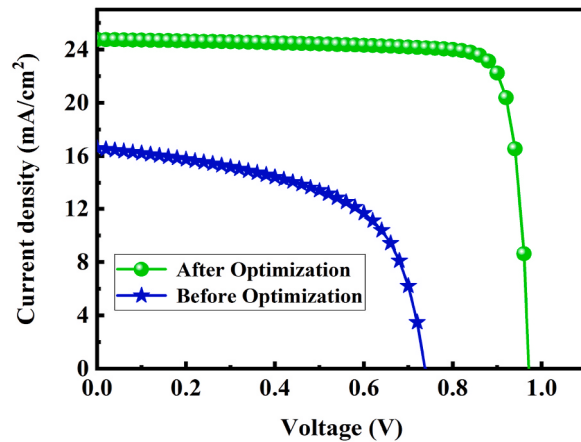


Fig. 11. After and before optimization the J-V curve.

4. Conclusion

In conclusion, this research presents the results of a numerical analysis of a highly reliable low bandgap MASnI₃-based PSCs in n-i-p hetero-junction with various material characteristics. We found that a significant boost in efficiency can result from a reduction in the concentration of doping. We also investigated the impact of different parameters to improved performance. We found that a significant boost in efficiency can result from change ETM. Finally, it was discussed how the WS₂ inter-layer enhanced the solar cells efficiency. The results of this work will help scientists create new perovskite materials for cutting-edge electrical and solar applications.

This research paper presents findings from an investigation into Performance Optimization of MASnI₃ Perovskite Solar Cells: Insights into Device Architecture. Through rigorous analysis and interpretation of lead-free solar cells we aim to contribute to the understanding of Performance Optimization of MaSnI₃ Perovskite Solar Cells: Insights into Device Architecture and its implications for

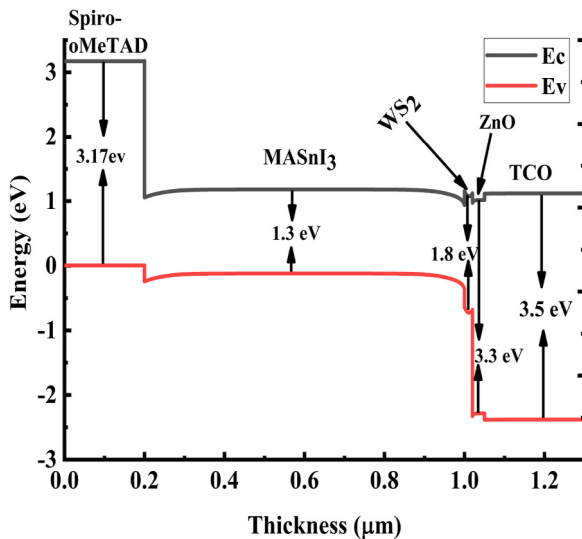


Fig. 12. MASnI₃ PSCs final energy band diagram.

solar cells. Our study underscores the importance of efficiency and provides insights that may inform future research, policy-making, or practical applications in lead free perovskite solar cells. We hope this paper stimulates further discussion and exploration in the field of lead free MASnI₃ based perovskite solar cells.

CRediT authorship contribution statement

Prithick Saha: Writing – original draft. **Sangeeta Singh:** Supervision. **Sanjib Bhattacharya:** Supervision.

Declaration of competing interest

We would like to declare no conflict of interest.

Data availability

No data was used for the research described in the article.

References

- [1] Z. Wang, Q. Lin, F.P. Chmiel, N. Sakai, L.M. Herz, H.J. Snaith, Efficient ambient-air-stable solar cells with 2D–3D heterostructured butylammonium-caesium-formamidinium lead halide perovskites, *Nat. Energy* 2 (9) (2017) 1–10.
- [2] Y. Liu, Z. Yang, D. Cui, X. Ren, J. Sun, X. Liu, J. Zhang, Q. Wei, H. Fan, F. Yu, X. Zhang, Two-inch-sized perovskite CH₃NH₃PbX₃ (X= Cl, Br, I) crystals: growth and characterization, *Adv. Mater.* 27 (35) (2015) 5176–5183.
- [3] Q. Lin, A. Armin, R.C.R. Nagiri, P.L. Burn, P. Meredith, Electro-optics of perovskite solar cells, *Nat. Photonics* 9 (2) (2015) 106–112.
- [4] A. Kojima, K. Teshima, Y. Shirai, T. Miyasaka, Organometal halide perovskites as visible-light sensitizers for photovoltaic cells, *J. Am. Chem. Soc.* 131 (17) (2009) 6050–6051.
- [5] NREL Efficiency Chart 2021, <https://www.nrel.gov/pv/cell-efficiency.html>, Apr. 2022.
- [6] Q. Jiang, Y. Zhao, X. Zhang, X. Yang, Y. Chen, Z. Chu, Q. Ye, X. Li, Z. Yin, J. You, Surface passivation of perovskite film for efficient solar cells, *Nat. Photonics* 13 (7) (2019) 460–466.
- [7] W. Ke, C.C. Stoumpos, I. Spanopoulos, L. Mao, M. Chen, M.R. Wasielewski, M.G. Kanatzidis, Efficient lead-free solar cells based on hollow en MASnI₃ perovskites, *J. Am. Chem. Soc.* 139 (41) (2017) 14800–14806.
- [8] T.B. Song, T. Yokoyama, J. Logsdon, M.R. Wasielewski, S. Aramaki, M.G. Kanatzidis, Piperazine suppresses self-doping in CsSnI₃ perovskite solar cells, *ACS Appl. Energy Mater.* 1 (8) (2018) 4221–4226.
- [9] W. Ke, C.C. Stoumpos, M. Zhu, L. Mao, I. Spanopoulos, J. Liu, O.Y. Kontsevoi, M. Chen, D. Sarma, Y. Zhang, M.R. Wasielewski, Enhanced photovoltaic performance and stability with a new type of hollow 3D perovskite en FASnI₃, *Sci. Adv.* 3 (8) (2017) e1701293.
- [10] Nakita K. Noel, et al., Lead-free organic-inorganic tin halide perovskites for photovoltaic applications, *Energy Environ. Sci.* 7 (9) (2014) 3061–3068.
- [11] M. Aldamasy, Z. Iqbal, G. Li, J. Pascual, F. Alharthi, A. Abate, M. Li, Challenges in tin perovskite solar cells, *Phys. Chem. Chem. Phys.* 23 (41) (2021) 23413–23427.
- [12] N. Jaiswal, V.P. Singh, C.P. Singh, D. Punetha, S.K. Pandey, Development of Solution-Processed Eco-Friendly Cs₂SnI₆ Double Perovskite Thin-Film Solar Cell, in, *IEEE J. Photovolt.* 14 (2) (2024) 265–271, <https://doi.org/10.1109/JPHOTOV.2023.3343559>.
- [13] S. Prabhu, N. Pandey, D. Punetha, S. Chakrabarti, A comparative study of Cu₂ZnSn(S_xSe_{1-x})₄ nanoparticles for solar cells: from chemical synthesis to devices, *Mater. Today Commun.* 37 (2023) 106905.
- [14] Poonam Subudhi, Deepak Punetha, Pivotal avenue for hybrid electron transport layer-based perovskite solar cells with improved efficiency, *Sci. Rep.* 13 (1) (2023) 19485.
- [15] N. Pandey, S. Prabhu, D. Punetha, M.R. Mantri, S. Chakrabarti, Surfactant free, easy, low cost, and large scale hydrothermal synthesis and characterization of CZTS ink for photovoltaic utility, in: *New Concepts in Solar and Thermal Radiation Conversion V*, vol. 12668, SPIE, 2023, pp. 53–57.

- [16] D. Kumari, N. Jaiswal, R. Shukla, D. Punetha, S.K. Pandey, Design and fabrication of all-inorganic transport materials-based Cs_2SnI_6 perovskite solar cells, *J. Mater. Sci. Mater. Electron.* 34 (25) (2023) 1792.
- [17] R. Shukla, D. Punetha, R.R. Kumar, S.K. Pandey, Examining the performance parameters of stable environment friendly perovskite solar cell, *Opt. Mater.* 143 (2023) 114124.
- [18] A. Kumar, D. Punetha, S. Chakrabarti, Performance optimization of phenylethylammonium-formamidinium tin iodide perovskite solar cell by contrasting various ETL and HTL materials, *J. Nanoparticle Res.* 25 (3) (2023) 52.
- [19] R. Shukla, R.R. Kumar, D. Punetha, S.K. Pandey, Design perspective, fabrication, and performance analysis of formamidinium tin halide perovskite solar cell, *IEEE Journal of Photovoltaics* 13 (3) (2023) 404–410, <https://doi.org/10.1109/JPHOTOV.2023.3241793>.
- [20] R. Chandel, D. Punetha, D. Dhawan, N. Gupta, Optimization of highly efficient and eco-friendly EA-substituted tin based perovskite solar cell with different hole transport material, *Opt. Quant. Electron.* 54 (6) (2022) 337.
- [21] F. Hao, C.C. Stoumpos, D.H. Cao, R.P. Chang, M.G. Kanatzidis, Lead-free solid-state organic–inorganic halide perovskite solar cells, *Nat. Photonics* 8 (6) (2014) 489–494.
- [22] F. Hao, C.C. Stoumpos, R.P. Chang, M.G. Kanatzidis, Anomalous band gap behavior in mixed Sn and Pb perovskites enables broadening of absorption spectrum in solar cells, *J. Am. Chem. Soc.* 136 (22) (2014) 8094–8099.
- [23] F. Li, C. Zhang, J.H. Huang, H. Fan, H. Wang, P. Wang, C. Zhan, C.M. Liu, X. Li, L.M. Yang, Y. Song, A cation-exchange approach for the fabrication of efficient methylammonium tin iodide perovskite solar cells, *Angew. Chem. Int. Ed.* 58 (20) (2019) 6688–6692.
- [24] P. Umari, E. Mosconi, F. De Angelis, Relativistic GW calculations on $\text{CH}_3\text{NH}_3\text{PbI}_3$ and $\text{CH}_3\text{NH}_3\text{SnI}_3$ perovskites for solar cell applications, *Sci. Rep.* 4 (1) (2014) 4467.
- [25] T. Yokoyama, D.H. Cao, C.C. Stoumpos, T.B. Song, Y. Sato, S. Aramaki, M.G. Kanatzidis, Overcoming short-circuit in lead-free $\text{CH}_3\text{NH}_3\text{SnI}_3$ perovskite solar cells via kinetically controlled gas–solid reaction film fabrication process, *J. Phys. Chem. Lett.* 7 (5) (2016) 776–782.
- [26] F. Hao, C.C. Stoumpos, P. Guo, N. Zhou, T.J. Marks, R.P. Chang, M.G. Kanatzidis, Solvent-mediated crystallization of $\text{CH}_3\text{NH}_3\text{SnI}_3$ films for heterojunction depleted perovskite solar cells, *J. Am. Chem. Soc.* 137 (35) (2015) 11445–11452.
- [27] Y. Chen, T. Chen, L. Dai, Layer by layer growth of $\text{CH}_3\text{NH}_3\text{PbI}_3\text{-xCl}_x$ for highly efficient planar heterojunction perovskite solar cells, *Adv. Mater.* 27 (6) (2015) 1053–1059.
- [28] M. Weiss, J. Horn, C. Richter, D. Schlettwein, Preparation and characterization of methylammonium tin iodide layers as photovoltaic absorbers, *Phys. Status Solidi* 213 (4) (2016) 975–981.
- [29] M. Burgelman, P. Nollet, S. Degraeve, Modelling polycrystalline semiconductor solar cells, *Thin Solid Films* 361 (2000) 527–532.
- [30] R. Hock, T. Mayer, W. Jaegermann, P-type doping of spiro-oMeOTAD with WO_3 and the Spiro-MeOTAD/ WO_3 interface investigated by synchrotron-induced photoelectron spectroscopy, *J. Phys. Chem. C* 116 (34) (2012) 18146–18154.
- [31] S.A. Rutledge, A.S. Helmy, Carrier mobility enhancement in poly (3, 4-ethylenedioxythiophene)-poly (styrenesulfonate) having undergone rapid thermal annealing, *J. Appl. Phys.* 114 (13) (2013).
- [32] K.D. Jayan, V. Sebastian, Comprehensive device modelling and performance analysis of MASnI_3 based perovskite solar cells with diverse ETM, HTM and back metal contacts, *Sol. Energy* 217 (2021) 40–48.
- [33] Q.Y. Chen, Y. Huang, P.R. Huang, T. Ma, C. Cao, Y. He, Electro negativity explanation on the efficiency-enhancing mechanism of the hybrid inorganic–organic perovskite ABX_3 from first-principles study, *Chin. Phys. B* 25 (2) (2015) 027104.
- [34] P. Saha, S. Singh, S. Bhattacharya, Efficient and lead-free perovskite solar cells based on defect-ordered methyl ammonium antimony iodide, *IEEE Trans. Electron. Dev.* 70 (3) (2023) 1095–1101.
- [35] M.S. Uddin, M.K. Hossain, M.B. Uddin, G.F. Toki, M. Ouladsmane, M.H. Rubel, D.I. Tishkevich, P. Sasikumar, R. Haldhar, R. Pandey, An in-depth investigation of the combined optoelectronic and photovoltaic properties of lead-free $\text{Cs}_2\text{AgBiBr}_6$ double perovskite solar cells using DFT and SCAPS-1D frameworks, *Adv. Electr. Mater.* (2024) 2300751.
- [36] S. Bouhmaidi, M.B. Uddin, R.K. Pingak, S. Ahmad, M.H.K. Rubel, A. Hakamy, L. Setti, Investigation of heavy thallium perovskites TlGeX_3 ($X = \text{Cl}, \text{Br}$ and I) for optoelectronic and thermoelectric applications: a DFT study, *Mater. Today Commun.* 37 (2023) 107025.
- [37] M.K. Hossain, G.I. Toki, D.P. Samajdar, M. Mushtaq, Deep insights into the coupled optoelectronic and photovoltaic analysis of lead-free CsSnI_3 perovskite-based solar cell using DFT calculations and SCAPS-1D simulations, *ACS Omega* 8 (25) (2023) 22466–22485.
- [38] M.K. Hossain, G.I. Toki, A. Kuddus, M.H.K. Rubel, M.M. Hossain, H. Bencherif, M.F. Rahman, M.R. Islam, M. Mushtaq, An extensive study on multiple ETL and HTL layers to design and simulation of high-performance lead-free CsSnCl_3 -based perovskite solar cells, *Sci. Rep.* 13 (1) (2023) 2521.
- [39] M.K. Hossain, D.P. Samajdar, R.C. Das, A.A. Arnab, M.F. Rahman, Design and simulation of $\text{Cs}_2\text{BiAgI}_6$ double perovskite solar cells with different electron transport layers for efficiency enhancement, *Energy Fuel.* 37 (5) (2023) 3957–3979.
- [40] M.K. Hossain, A.A. Arnab, R.C. Das, K.M. Hossain, M.H.K. Rubel, Combined DFT, SCAPS-1D, and wxAMPS frameworks for design optimization of efficient $\text{Cs}_2\text{BiAgI}_6$ -based perovskite solar cells with different charge transport layers, *RSC Adv.* 12 (54) (2022) 35002–35025.
- [41] M.K. Hossain, M.K. Mohammed, R. Pandey, A.A. Arnab, M.H.K. Rubel, Hossain, Numerical analysis in DFT and SCAPS-1D on the influence of different charge transport layers of CsPbBr_3 perovskite solar cells, *Energy Fuel.* 37 (8) (2023) 6078–6098.
- [42] D. Ju, X. Jiang, H. Xiao, X. Chen, X. Hu, X. Tao, Narrow band gap and high mobility of lead-free perovskite single crystal Sn-doped $\text{MA}_3\text{Sb}_2\text{I}_9$, *J. Mater. Chem. A* 6 (42) (2018) 20753–20759.
- [43] S.J. Lee, S.S. Shin, Y.C. Kim, D. Kim, T.K. Ahn, J.H. Noh, J. Seo, S.I. Seok, Fabrication of efficient formamidinium tin iodide perovskite solar cells through SnF_2 –pyrazine complex, *J. Am. Chem. Soc.* 138 (12) (2016) 3974–3977.
- [44] N. Lakhdar, A. Hima, Electron transport material effect on performance of perovskite solar cells based on $\text{CH}_3\text{NH}_3\text{GeI}_3$, *Opt. Mater.* 99 (2020) 109517.
- [45] F. Azri, A. Meftah, N. Sengouga, A. Meftah, Electron and hole transport layers optimization by numerical simulation of a perovskite solar cell, *Sol. Energy* 181 (2019) 372–378.
- [46] X. Liu, K. Yan, D. Tan, X. Liang, H. Zhang, W. Huang, Solvent engineering improves efficiency of lead-free tin-based hybrid perovskite solar cells beyond 9, *ACS Energy Lett.* 3 (11) (2018) 2701–2707.
- [47] Y. Guo, J. Jiang, S. Zuo, F. Shi, J. Tao, Z. Hu, X. Hu, G. Hu, P. Yang, J. Chu, RF sputtered CdS films as independent or buffered electron transport layer for efficient planar perovskite solar cell, *Sol. Energy Mater. Sol. Cells* 178 (2018) 186–192.
- [48] W. Qiu, M. Buffiere, G. Brammertz, U.W. Paetzold, L. Froyen, P. Heremans, D. Cheyns, High efficiency perovskite solar cells using a PCBM/ZnO double electron transport layer and a short air-aging step, *Org. Electron.* 26 (2015) 30–35.
- [49] S. Chatterjee, A.J. Pal, Introducing Cu_2O thin films as a hole-transport layer in efficient planar perovskite solar cell structures, *J. Phys. Chem. C* 120 (2016) 1428–1437.
- [50] T. Minemoto, M. Murata, Theoretical analysis on effect of band offsets in perovskite solar cells, *Sol. Energy Mater. Sol. Cell.* 133 (2015) 8–14.
- [51] M. Patel, P.M. Pataniya, V. Patel, C.K. Sumesh, D.J. Late, Large area, broadband and highly sensitive photodetector based on $\text{ZnO-WS}_2/\text{Si}$ heterojunction, *Sol. Energy* 206 (2020) 974–982.
- [52] N. Balis, E. Stratakis, E. Kymakis, Graphene and transition metal dichalcogenide nanosheets as charge transport layers for solution processed solar cells, *Mater. Today* 19 (10) (2016) 580–594.
- [53] K. Wu, H. Ma, Y. Gao, W. Hu, J. Yang, Highly-efficient heterojunction solar cells based on two-dimensional telluride and transition metal dichalcogenides, *J. Mater. Chem. A* 7 (13) (2019) 7430–7436.
- [54] P. Saha, S. Singh, S. Bhattacharya, Higher efficiency and stability in planar homojunction hybrid antimony ($\text{MA}_3\text{Sb}_2\text{I}_9$) based perovskite solar cells, in: *IEEE Journal of Quantum Electronics*, 2023.
- [55] P.S. Chandrasekhar, V.K. Komarala, Graphene/ZnO nanocomposite as an electron transport layer for perovskite solar cells:the effect of graphene concentration on photovoltaic performance, *RSC Adv.* 7 (46) (2017) 28610–28615.
- [56] Y.E. Lye, K.Y. Chan, Z.N. Ng, A review on the progress, challenges, and performances of tin-based perovskite solar cells, *Nanomaterials* 13 (3) (2023) 585.